Applied Surface Science 638 (2023) 158012

Contents lists available at ScienceDirect

Applied Surface Science

journal homepage: www.elsevier.com/locate/apsusc

Full Length Article

Development of ultrasensitive new sensors based on thio-functionalized heterogeneous layers of gold/graphene/copper for glucose detection

Chawki Awada [a], Hassan H. Hammud [b,*], Hawra A. Bukhamsin [b], Dolayl E. Al-Hudairi [b], Francesco Ruffino [c,*]

[a] Department of Physics, College of Science, King Faisal University, P.O. Box 400, Al Ahsa 31982, Saudi Arabia
[b] Department of Chemistry, College of Science, King Faisal University, P.O. Box 400, Al-Ahsa 31982, Saudi Arabia
[c] Dipartimento di Fisica e Astronomia "Ettore Majorana"-Università di Catania and CNR-IMM, Catania (University) Unit, via S. Sofia 64, 95123 Catania, Italy

ARTICLE INFO

Keywords:
Glucose
Gold nanoparticles
4-NTP
Impedance
Cyclic voltammetry
Raman spectroscopy

ABSTRACT

In this work, we report for the first time a new electro-chemical sensors based on (4-Nitrothiophenol) 4-NTP functionalized heterogeneous layers of gold/graphene/Cu for highly sensitive detection of glucose. 4-NTP molecules were immobilized into the surface of gold nanostructures. Surface enhanced Raman scattering was performed in order to assure of the 4-NTP bonding and the optical enhancement of gold nanostructures. SERS intensities generated by the new sensors confirm the presence of active catalytic sites rich with charges. The electrochemical measurement performed for glucose using cyclic voltammetry showed an increasing of sensitivity 3 times faster in the case of functionalized sensors than the standard ones. Nyquist plot proved a decrease in the impedance for glucose with the presence of 4-NTP into the surface. Due to the 4-NTP molecules attached to their surface, the new sensors were proved to be higher sensitive for the detection of glucose. The sensitivity obtained by cyclic voltametric techniques was 179.6 μA/mM.cm^2 and 420.8 μA/mM.cm^2 for electrode 1 and 2 respectively. The dynamic range is 2.0–19.6 mM (36.0—353.2 mg/dL) of glucose for electrode 1 while it is 2.0–29.1 mM (36.0–524.9 mg/dL) of glucose for electrode 2. The lower detection limit is thus 0.5 mM (9.0 mg/dL) the same for both electrodes. The electrode was also tested as glucose sensor using electrochemical impedance spectroscopy (EIS) techniques.

1. Introduction

Fast, sensitive and selective sensing of glucose are important issues in many scientific and technological fields including health, food and environmental monitoring [1–3]. The non-enzymatic electrochemical sensing devices allow several advantages, such as high stability, cost-effective production, adaptability to broad range of working conditions [4]. Several classes of nanostructures supported onto carbon nanotubes and graphene were, recently, proposed to design biosensors with fast response, high sensitivity, high stability and being user-friendly [5,6]. In this regard, several nanostructured non-enzymatic electrochemical glucose sensors are based on nanostructures of 4d and 5d blocks metals such as Au due to its high electrocatalytic activity [7]. For example, nanostructured Au surfaces exhibit high electrocatalytic activity towards glucose oxidation while, conversely, to flat Au surfaces, do not exhibit activity [7]. Generally, in addition, the substrate used for the realization of the electrochemical sensing electrode represents an important issue. The advantages of carbon materials used as substrate include low cost, wide potential window, and the possibility of a variety of chemical functionalization [8].

In particular, graphene (Gr) is an ideal substrate material for Au nanostructures to be used as electrocatalysists, mainly due to its high electrical conductivity and large electrochemical potential window (~2.5 V in 0.1 mM phosphate buffered saline) [9]. Recently, a number of works have demonstrated that graphene-nanoparticle hybrid structures can act synergistically to offer a number of unique physicochemical properties advantageous for sensing applications [10]. Athough the progress observed in their sensitibty properties, no one has reported functionalized heterogenous layers of gold/graphene/copper (Au/Gr/Cu) with thiol group to detect glucose.

Hence, in this work, a new sensor based on 4-Nitrothiophenol (4-NTP) functionalized gold/graphene/copper (Au/Gr/Cu) is developed for highly selective and sensitive electrochemical detection of glucose. The Au film was deposited, on the Gr surface, supported on Cu foil, via

* Corresponding authors.
E-mail addresses: hhammoud@kfu.edu.sa (H.H. Hammud), francesco.ruffino@ct.infn.it (F. Ruffino).

https://doi.org/10.1016/j.apsusc.2023.158012
Received 8 May 2023; Received in revised form 30 June 2023; Accepted 10 July 2023
Available online 10 July 2023

the sputtering method. 4-NTP molecules were attached onto the Au surface by means of their thiol group. Scanning electron microscopy (SEM) was used to study the topography of the sensors. Surface Enhanced Raman Scattering (SERS) spectra were performed to check the 4-NTP adsorption and to verify the optical enhancement produced by the Au/Gr layers. Electrochemical studies, by using cyclovoltamogram (CV) and impedance measurements, were performed on Au/Gr/Cu without 4-NTP and with 4-NTP to investigate the effect of 4-NTP molecules on the sensitivity of detection for glucose.

2. Experimental section

2.1. Characterization methods

The samples surface morphology was studied by scanning electron microscopy (SEM) analyses using a Zeiss FEG-SEM Supra 25 Microscope operating at 5 kV.

Raman spectra were collected using a confocal Raman microscope (LabRAM HR800, Horiba Scientific, Villeneuve-D'Ascq, France) in a backscattering geometry with a spectral resolution of 0.23 cm^{-1} at ambient temperature. A He–Ne Laser of $\lambda = 632.8$ nm with an output power of 2 mW was used for the Raman measurement. An objective of 50X, a grating of 1800 L/mm, and a selected power of 500 μW were used for SERS measurement.

Electrochemical cyclic voltammetry and impedance measurements were carried out by the instrument Gamry potentiostat/galvanostat/ZRA Reference 600 having software v7. The three-electrode cell used contained: (1) counter electrode (platinum wire 0.5 mm), (2) reference electrode (saturated silver - silver chloride electrode (sat. Ag/AgCl)) and (3) a working electrode: unmodified nanogold (1) or thiol modified nanogold electrode (2) as described before. Electrode (1) consists of nanogold/graphene/copper film (Au-7.5 nm/Gr/Cu) while modified electrode (2) consists of 4-nitrothiophenol/nanogold/graphene/copper film (4-NTP/Au-7.5 nm/Gr/Cu). In each case, the film electrode, with area of about 0.25 cm^2, was mounted on a silver wire (1 mm diameter) to provide electrical connection with the potentiostat. The electrolyte used was a 0.5 M NaOH solution. In the impedance measurement, a sinusoidal voltage perturbation of amplitude 10 mV rms was applied in the frequency range 100 kHz − 0.1 Hz with 10 points/decade.

2.2. Fabrication and functionalization

Single layer graphene sheets on Cu substrate were acquired by graphene-supermarket (Graphene supermarket, Ronkonkoma, USA). The single-layer graphene film is continuous across copper surface steps and grain boundaries. The Au depositions were performed onto the graphene slides by means of a RF Emitech K550X sputter coater apparatus, clamping the substrates against the cathode located straight opposite the target source (99.999% purity target). The electrodes were laid at a distance of 40 mm under Ar flow keeping a pressure of 0.02 mbar in the chamber. During the depositions, the working current and the deposition time were set to obtain an effective thickness for the deposited Au films of 7.5 nm as checked by subsequent ex-situ Rutherford backscattering analyses performed using 2 MeV $^4He^+$ backscattered ions at 165° (with a statistical error of 5%).

The Au/Gr/Cu film was immersed in a 10^{-3} M solution of 4-NTP prepared in ethanol absolute. In order to assure a complete bonding between 4-NTP molecules and Au toward thiol group, we immersed the substrate for 24 h. The substrates were rinsed with ethanol to remove the non-bonded molecules and then used for SERS measurements.

3. Results and discussion

3.1. Structural analysis

Fig. 1 (a)-(b) report SEM image of Cu/graphene bare surface; while (c)-(d) report SEM micrographs of the surface of the Au film as-deposited on the Cu/Gr substrate, with increasing magnification from (c) to (d). In these images, the Au surface morphology appears to have a quasi-continuous percolating structure typical of a metal film in the late stage of growth on a non-wetting substrate [11], the surface-free energy of Au is $\gamma_{Au} = 1.537$ J/m^2 [12], the surface-free energy of graphene is $\gamma_{GR} = 0.0467$ J/m^2 [13]. After the Au clusters nucleation and growth, the coalescence stage starts and, then, the formation of larger compact islands is accompanied by a wiping action in which part of the substrate which was covered initially is wiped clean. This results in a distribution of larger islands on the substrate, separated by gaps between them.

3.2. SERS study

Optical images show the color contrast difference between Cu/Gr and 4-NTP functionalized gold/Gr/Cu, see Fig. 2a, b. In Cu/Gr, pink color of Cu is clearly observed, however, in Au/Gr/Cu, the color is less pronounced and with more boundaries. Raman spectra are measured on the graphene layer, see Fig. 2c. We observe G and 2D bands located at 1578 cm^{-1} and 2633 cm^{-1}, respectively. The ratio $I_{2D}/I_G \sim 2.6$ confirms the presence of a graphene monolayer. Raman spectra are also acquired on 4-NTP functionalized Au/Gr/Cu in order to confirm its chemical adsorption into Au surface. C–H, C-N, NO_2, and C–C are the vibrational modes of 4-NTP located at 1080 cm^{-1}, 1110 cm^{-1}, 1337 cm^{-1}, and 1574 cm^{-1}, respectively, see Fig. 2d. 2D band disappears when a 7.5 nm of gold is deposited, the latter could be explained by the absorption of light by the gold layer. In fact, the Raman intensity of vibrational modes attributed to 4-NTP is amplified by the localized–electrical field enhanced by Au nanostructures [14,15]. Two enhancement factors can contribute to the amplification of Raman signal, the chemical and the optical enhancement. The first one is due to the charge transfer between the molecules and the Gold/Graphene layers. The optical enhancement could be due to the presence of hot spots generated from the interference of surface plasmon polaritons (SPPs) in to the fractal surface, see Fig. 1c, d. The optical enhancement can also be generated from the gap between gold nanoparticles. In fact, a monolayer of 4-NTP is formed into the gold surface, 4-NTP molecules bond towards its sulfur atom with gold. The latter has been reported in different studies [16,17]. In conclusion, at ambient temperature, a 4-NTP layer is formed into surface without any dimerization effect.

3.3. Electrochemical study

Cyclic voltammetry (CV) was conducted in a 0.5 M NaOH solution to investigate the electrocatalytic activity of nano-gold electrodes. Unmodified nano-gold electrode (1) (Au-7.5 nm/Gr/Cu) or thiol modified nano-gold electrode (2) (4-NTP/Au-7.5 nm/Gr/Cu) were used as working electrodes in order to explore the electro-oxidation of glucose. The CV was measured in the potential window (-0.5 V to + 0.8 V or − 1.0 V to + 1.0 V) vs. sat Ag/AgCl with a scan rate of 50 mV/s in 0.5 M NaOH medium, in the presence or absence of glucose with concentration ranging from (2.0 mM to 33.8 mM).

3.3.1. Behavior of electrodes in basic NaOH medium

Fig. 3 shows the voltammogram for the Au nanoparticles deposited on the graphene supported on copper foil (electrode 1), and for the thiol-gold nanoparticles deposited on the graphene supported on copper foil (electrode 2) [18]. The structure of the nanoparticles was maintained by avoiding the oxidation of the surface at high potential. For that reason, the upper potential limit is set below 1.2 V, since the oxidation/reduction cycles may change the surface structure of the Au electrodes [18,19]. Three anodic peaks (A1, A2, A2 shoulder and A3) were observed for electrode 1 and 2 on the positive scan before the onset of the surface oxidation, Table 1. A1 and A2 peaks are due to the adsorption of OH^- on the electrode surface and formation of Au-OH species [19]. Peak A3 is related to the oxidation of OH^-; at this peak potential

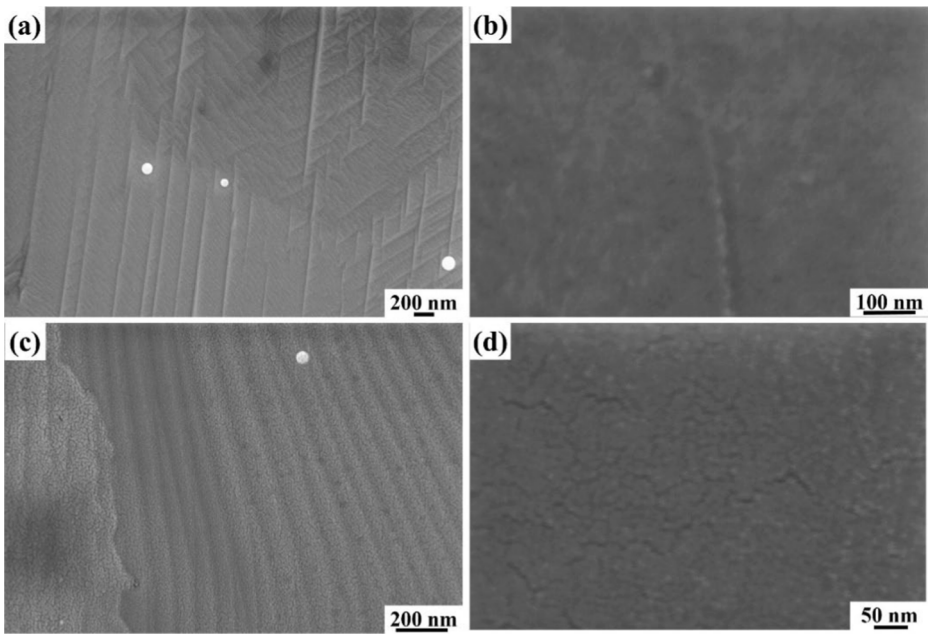

Fig. 1. (a)-(b) SEM images of the Cu/graphene bare surface, with increasing magnification from (a) to (b). (c)-(d) SEM images of the surface of the 7.5 nm-thick Au film as deposited on the Cu/graphene substrate, with magnification from (c) to (d).

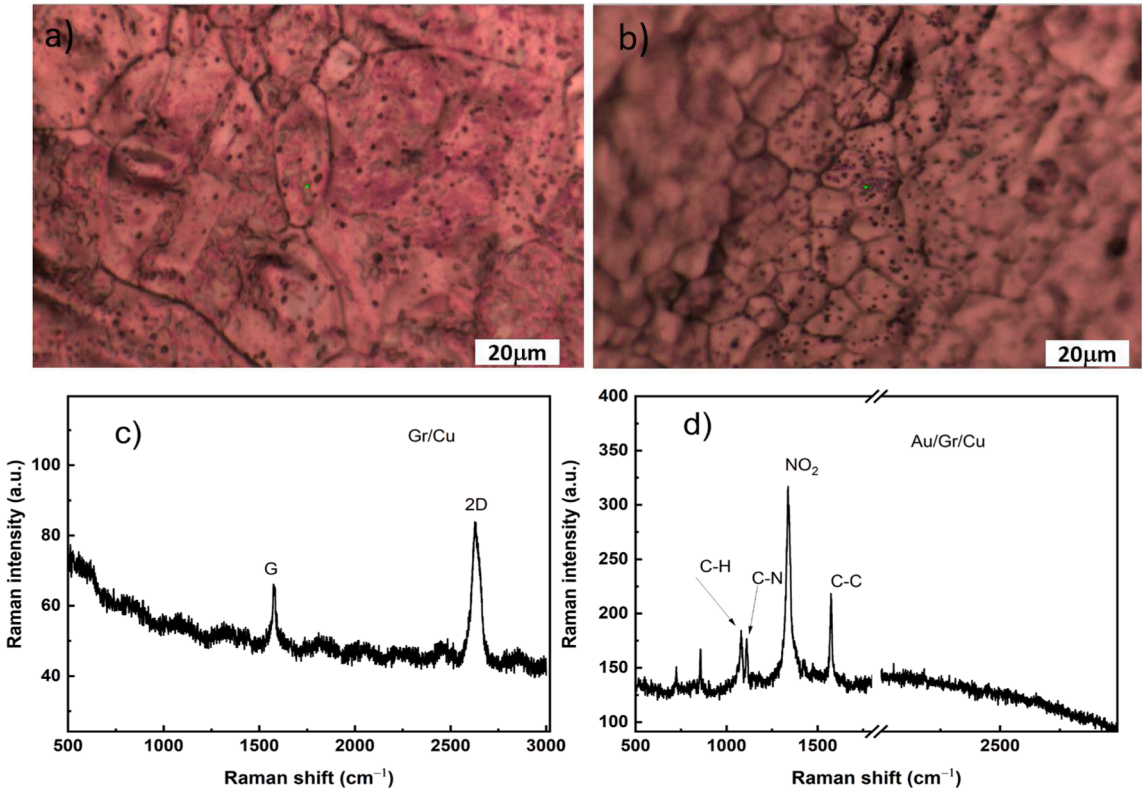

Fig. 2. a, b) optical image 50x of Gr/Cu and 7.5 nm Au/Gr/Cu. c, d) Raman spectra of Gr and 7.5 nm Au/Gr/Cu functionalized with 4-NTP, G and 2D bands of Gr are located at 1578 cm^{-1} and 2633 cm^{-1}, respectively. C–H, C-N, NO_2, and C–C are the vibrational modes of 4-NTP located at 1080 cm^{-1}, 1110 cm^{-1}, 1337 cm^{-1}, and 1574 cm^{-1}, respectively. Laser wavelength 632.8 nm, irradiated power 500 microwatt, 1800 gr/mm, 0.23 cm^{-1}, 5 s integration time for each spectra, each spectra is averaged over three different positions for both Gr and 4-NTP/Au/Gr/Cu.

value, OH^- adsorbed should have already covered a significant fraction of the surface. In addition, the upper potential is stopped at 1.0 V which is the onset of oxygen evolution peak in order to minimise its effect on A3 peak [20–22].

However, in the negative scan there are four peaks C3, C2, C1 and C0, Table 1. Peak C3 is the reduction of the oxidized products form OH^-. Peak C2 and C1 are due to the stripping reaction of hydroxide from the surface. Another peak C0 appeared at the lower scan limit. It can be attributed to the reduction of adsorbed (H^+).

In comparison electrode (1) showed smaller peak currents than

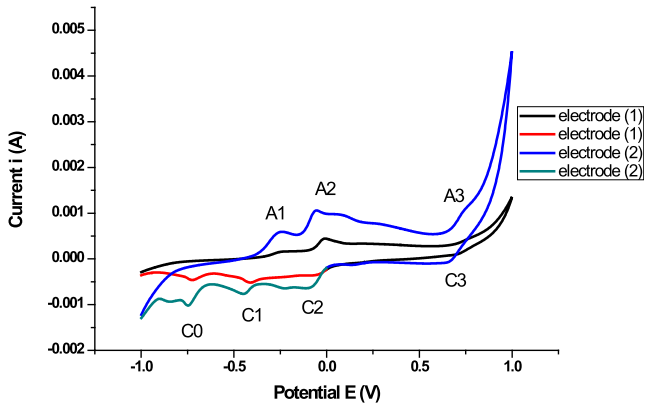

Fig. 3. Cyclic voltammogram in 0.5 M NaOH of nano gold electrode (1) and CA2 thiol modified nano-gold electrode (2). Scan rate: 50 mV s^{-1}.

electrode (2). The peaks current ratio for electrode (1) over (2), and the % increase in current of electrode (2) over (1) is presented in Table 1, for all anodic peaks (A1, A2, A2 sh., A3) and cathodic peaks (C0, C1, C2, C3). The % enhancement of electroactivity ranges from 39 to 74% depending on the peak. This indicates improvement of electrochemical activity of (2) compared to (1) due to that (2) has been successfully prepared by functionalized of (1) with thiol groups. Thus, incorporation of thiols group of nitro-thiophenol bind to gold nanoparticle while the nitro group attract OH^- to electrode surface through hydrogen bonds. This enhances the electroactivity of gold nanoparticles electrode for detection of glucose.

Supplementary Fig. S1 is the cyclic voltammogram of the starting substrate copper foil CA5 electrode which is further compared with graphene coated copper foil CA17, electrode. The latter is additionally modified by thiol, CA S17 electrode. While CA5 shows peaks A1, A2 and A3 (weak) in close region to the gold nanoparticles electrode (1) and (2), In CA17 the graphene has masked the electroactive copper surface, however the incorporation of thiol in CA S17 enhanced only peak C related to the electro-oxidation of hydroxyl ion OH^-.

3.3.2. *Behavior of electrodes in presence of glucose*

Cyclic voltammogram were recorded in the presence of different glucose concentrations (range 2.0 mM to 33.8 mM) in 0.5 M NaOH solution in order to assess the electro catalytic oxidation of glucose by the electrodes. Fig. 4a shows an overlay of cyclic voltammogram of nano-gold electrode (1) (blue) and thiol modified nano-gold electrode (2) (black) in the presence of 9.9 mM glucose. The thiol modified nano-gold electrodes (2) showed more increase in the all the anodic peaks A1, A2 and A3 compared to non-modified nano-gold electrode (1). This indicates better electro-catalytic activity of nano-gold electrode (2) toward glucose oxidation than electrode (1). The electro-oxidation of glucose by nano-gold in an alkaline medium can be simplified as: OH^- adsorption occurs at peak A1 and formation of Au-OH species which can be involved in the oxidation of glucose at higher potential. Peak A1 decreases as the glucose concentration increases since glucose can complex with gold and compete with OH^- adsorption on the surface of electrode and cause a decrease of exposed surface to OH^- [23], see Fig. 4b (electrode 1) and Fig. 4c (electrode 2) for the scan range − 1.0 V to 1.0 V; while Fig. SI 2a and Fig. SI 2b for the scan range − 0.5 V to + 0.8 V. Glucose oxidation occurs afterwards at peaks A2 and A3, since the currents at these peaks increase with increase in glucose concentration, and the gold metal is itself involved in the oxidation reaction. A2 appears as plateau in the case of electrode 2. At peak A2, glucose is oxidized into glucose carboxylic acid derivatives such as gluconic, glucuronic and glucaric acid anion [23,24]. Finally, peak A3 at about 780 mV for electrode 1 and 740 mV for electrode 2. There is a 40 mV negative shift for peak A3 for electrode 2 (with thiol) compared to electrode 1 (without thiol). This indicates that modification of gold nanoparticle electrode with thiol caused enhancement towards glucose sensing. Peak A3 is characterized by a much higher current density than peaks A1 and A2. It is present in the voltammograms of glucose using electrode 1 and 2. Peak A3 can be due to the cleavage of the C–C bond, which possibly take place at this high overpotentials. It is independent of the available functional groups such as hydroxyl or aldehydic group. This ultimately leads to the formation of lower carboxylic acids such as formic acid [24].

The effect of oxygen evolution which has for electrode 2 an onset potential of OER at 840 mV immediately after the glucose oxidation / breakage peak A3 at 740 mV, and has minor effect on A3 peak. For electrode 1 the OER onset potential is at 860 mV while A3 peak is at 780 mV [20–22]. However, the oxygen evolution peak depends on OH^- concentration which remained constant during the experiment of increasing concentration of glucose. Thus, its effect is the same for all concentration of glucose, and only increasing the concentration of glucose causing additional increase in the current [24–28].

The increase in the cathodic peak A2 and A3 for electrode (2) more than (1) can be attributed to the ease of oxidation of glucose by electrode (2). Thiol groups on gold nanoparticles interact with glucose molecules through hydrogen bonds, enhance adsorption of glucose on the electrode surface and thus facilitate oxidation of glucose.

Glucose having several hydroxyl groups can participate in H-bonds with nitro group of 4-NTP. The thiols RSH molecules were predicted to bind in a parallel fashion to gold surface [29]. The H-bond entrapment of glucose by the 4-NTP attached at the surface of gold nanoparticles bring the glucose in a closer position with the gold nanoparticles and thus facilitate electrons transfer for oxidation and sensing of glucose.

In the negative scan and at approximately 0.7 V, the peak is a weak reduction peak C3 at low concentration of glucose while it is changed onto an oxidation peak at high concentration of glucose. It can be also attributed to further oxidation of glucose involving C–C bonds cleavage. Another oxidation peak appeared at about 0.2 V in the negative scan and it is more prominent in the case of electrode (2). The peak current increases with increase in concentration of glucose. It can also involve oxidation of glucose to carboxylic acid derivatives. For all other cathodic peaks C2, C1 and C0, the peak current decreases with increase in glucose

Table 1
Cyclic voltammetry data peak currents and (potentials) for electrode (1) and (2) and % current (1)/ current (2) (% i(1)/i(2)) in 0.5 M NaOH, scan range from − 1.0 V to 1.0 V with as 50 mV/s scan rate.

	Anodic Peaks Current, mA (potential, mV)				**Cathodic Peaks Current, mA (potential, mV)**			
Peaks	A1	A2	A2 sh.	A3	C3	C2	C1	C0
Electrode (1)	0.1538 (-241.2)	0.4615 (-3.398)	0.3710 (71.35)	0.5158 (766.7)		−0.4121 (-110.8)	−0.5339 (410.6)	−0.5158 (730.5)
Electrode (2)	0.5882 (-240.1)	1.059 (-53.23)	1.005 (71.35)	1.131 (755.4)	−0.0996 (651.2)	−0.6787 (-107.6)	−0.8054 (-451.9)	−1.059 (-748.6)
% (i (1)/ i (2))	26.15%	43.58%	36.92%	45.61%		60.72%	66.29%	48.71%
% increase in i (2) over i (1)	73.85%	56.42%	63.08%	54.39%		39.28%	33.71%	51.29%

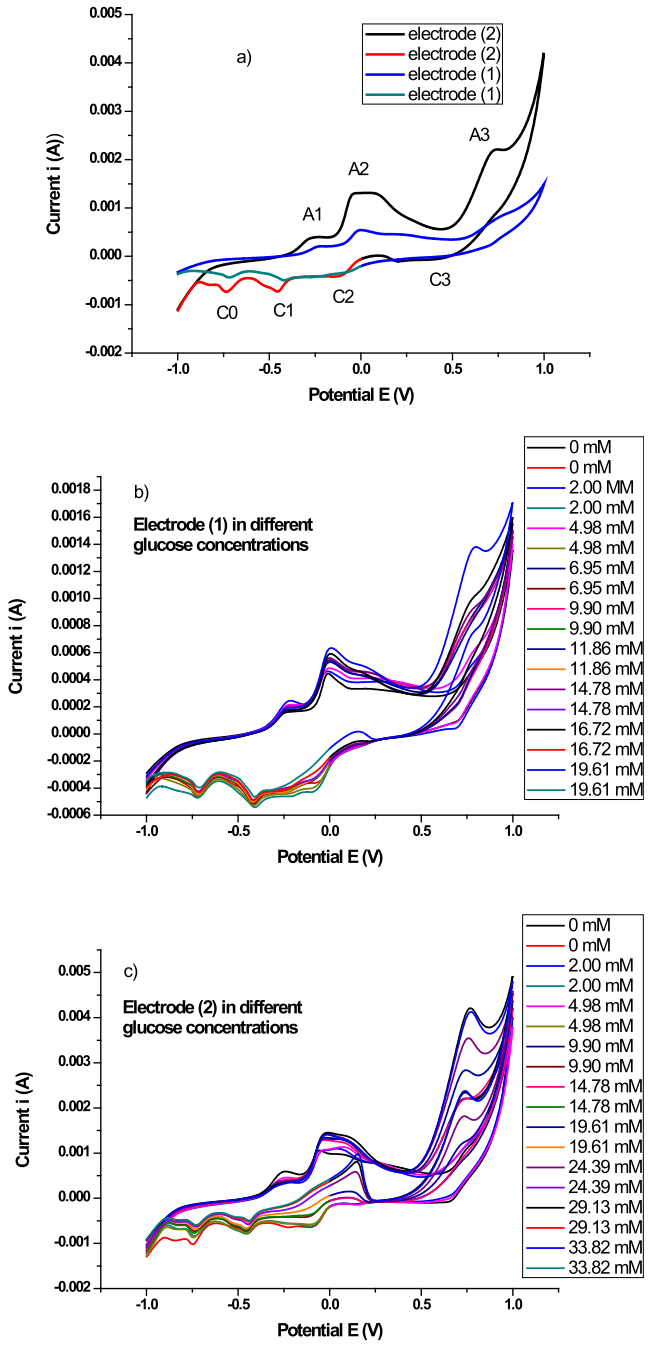

Fig. 4. (a) Comparison Cyclic voltammogram of nano gold electrode (1) and thiol modified nanogold electrode (2) in presence of 9.90 mM glucose and 0.5 M NaOH with a scan rate 50 mV.s^{-1}. (b) Effect of glucose concentration mM in 0.5 M NaOH solution at a scan rate of 50 mV using electrode (1) in the range − 1.0 to + 1.0 V (c) Effect of glucose concentration (mM) in 0.5 M NaOH solution at a scan rate of 50 mV.s^{-1} using modified electrode (2) in the range − 1.0 to + 1.0 V.

concentration. The C2 and C1 peaks can involve stripping of hydroxyl anion from the electrode surface. The peak current A3 is proportional to glucose concentration, Fig. 4b and c. Therefore, this method can be used as direct quantitative detection of glucose (Fig. 5a and b). The calibration curves show high correlation square coefficient R^2 of 0.981 and 0.982 for electrode 1 and 2 respectively. The sensitivity obtained was 0.0449 mA/mM and 0.1052 mA/mM or (179.6 μA/mM.cm^2 and 420.8 μA/mM.cm^2) for electrode 1 and 2 respectively. The dynamic range is 2.0–19.6 mM (36.0—353.2 mg/dL) for electrode 1 while it is 2.0–29.1

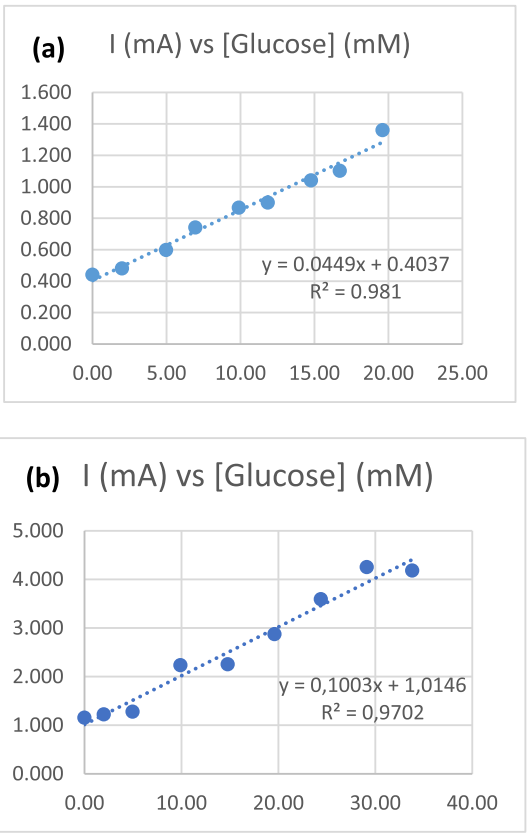

Fig. 5. (a) Calibration curve: Current I (mA) versus glucose concentration (mM) obtained from the oxidation peak A3 using electrode (1) in 0.5 M NaOH. **(b)** Calibration curve: Current I (mA) versus concentration of glucose (mM) obtained from the oxidation peak A3 using electrode (2) in 0.5 M NaOH.

mM (36.0–524.9 mg/dL) for electrode 2. The lower detection limits is thus 0.5 mM (9.0 mg/dL) the same for both electrodes. While exceeding the upper limit of concentration causes a slight decrease in the current. Such as for electrode 2, the current corresponding for 33.8 mM (609.1 mg/dL) glucose shows a slight decrease compared to the current for 29.1 mM (524.9 mg/dL) see Fig. 4c). Blood sugar level above 250 mg/L is considered very high, the upper limit (524.9 mg/dL) detected by electrode 2 can cover glucose in patients with severe diabetes.

CV peaks for electrochemical oxidation of glucose at different concentration mM, in the scan range − 1.0 to + 1.0 V were compared between electrodes (1) and (2), Fig. SI 3. It is noted that electrode (2) showed more intense peak currents than electrode (1).

3.3.3. *Scan rate's study*

In order to study the electrocatalytic reaction, cyclic voltammetry of the modified electrode (2) was recorded in the presence of glucose at different scan rates (Fig. 6a) [30]. Both the anodic peak currents *Epa* (A1, A2, A2 shoulder, A3) and the cathodic peaks currents *Epc* (C0, C1) increased as the scan rate SR increased. A positive shift was observed for *Epa* while a negative shift for *Epc* with increase in scan rate.

In addition, the electrochemical reaction of the modified electrode (2) is more controlled by diffusion process rather than by surface confinement. The correlation coefficient R^2 of the plot of peak current intensities against square root of scan rate $(SR)^{1/2}$ for peak A2 (0.9920) Fig. 6b; for peak A2 shoulder (0.9885) Fig. 6c; and for peak A3 (0.9545) Fig. 6d are greater than R^2 of the corresponding linear plots of current intensity vs scan rate SR (0.9640), (0.9345) and (0.8816), respectively [26,30].

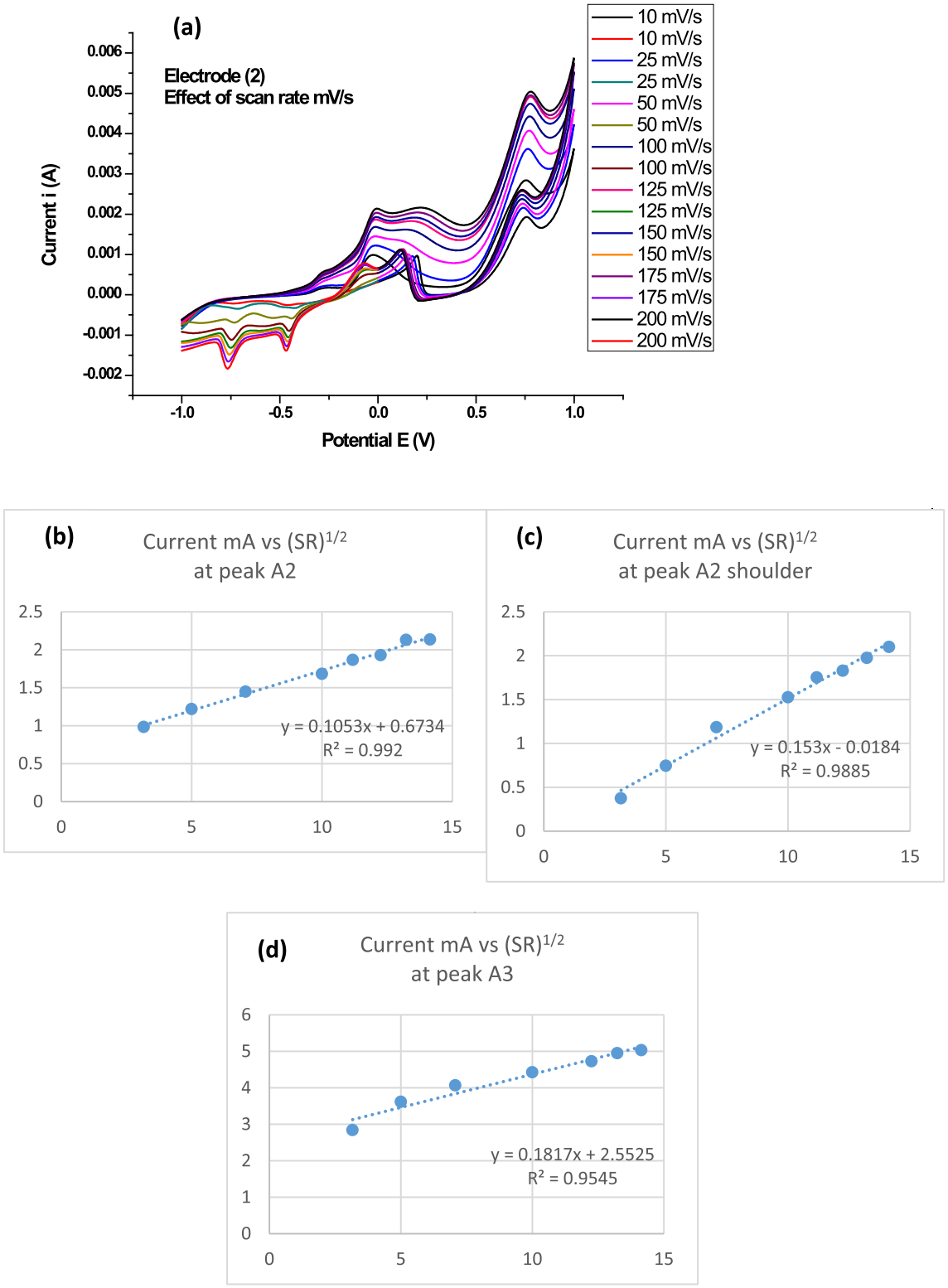

Fig. 6. Electrochemical oxidation of glucose (33.82 mM) in 10 mL NaOH (0.5 M) using electrode (2): (a) Cyclic voltammogram effect of scan rate mV/s (10, 25, 50, 100, 125, 150, 175, 200 mV/s); Plots of peak current intensities mA against sqrt (scan rate) $(mV)^{1/2}s^{-1/2}$ (b) for peak A2, (c) for peak A2 shoulder and (d) for peak A3.

3.3.4. Stability of electrode (2)

The stability of the thiol modified electrode (2) is tested using cyclic voltammetry after 100 consecutive cycles with a scan rate of 100 $V.s^{-1}$ in presence of glucose (33.82 mM) in 0.5 M NaOH (Fig. 7a) [27]. While it is noted that in Fig. 7b that the electroactivity of electrode after 100 cycles is not affected since the anodic peaks A1 and A2 did not drop in intensity at a scan rate 50 mV/s. While the A3 peaks which is related to oxidation of glucose into fragmented molecules has decreased in intensity. It can be observed that the anodic peak current intensity A3 at 780.4 mV after 100 cycles retained 85.54% of its original value. While it

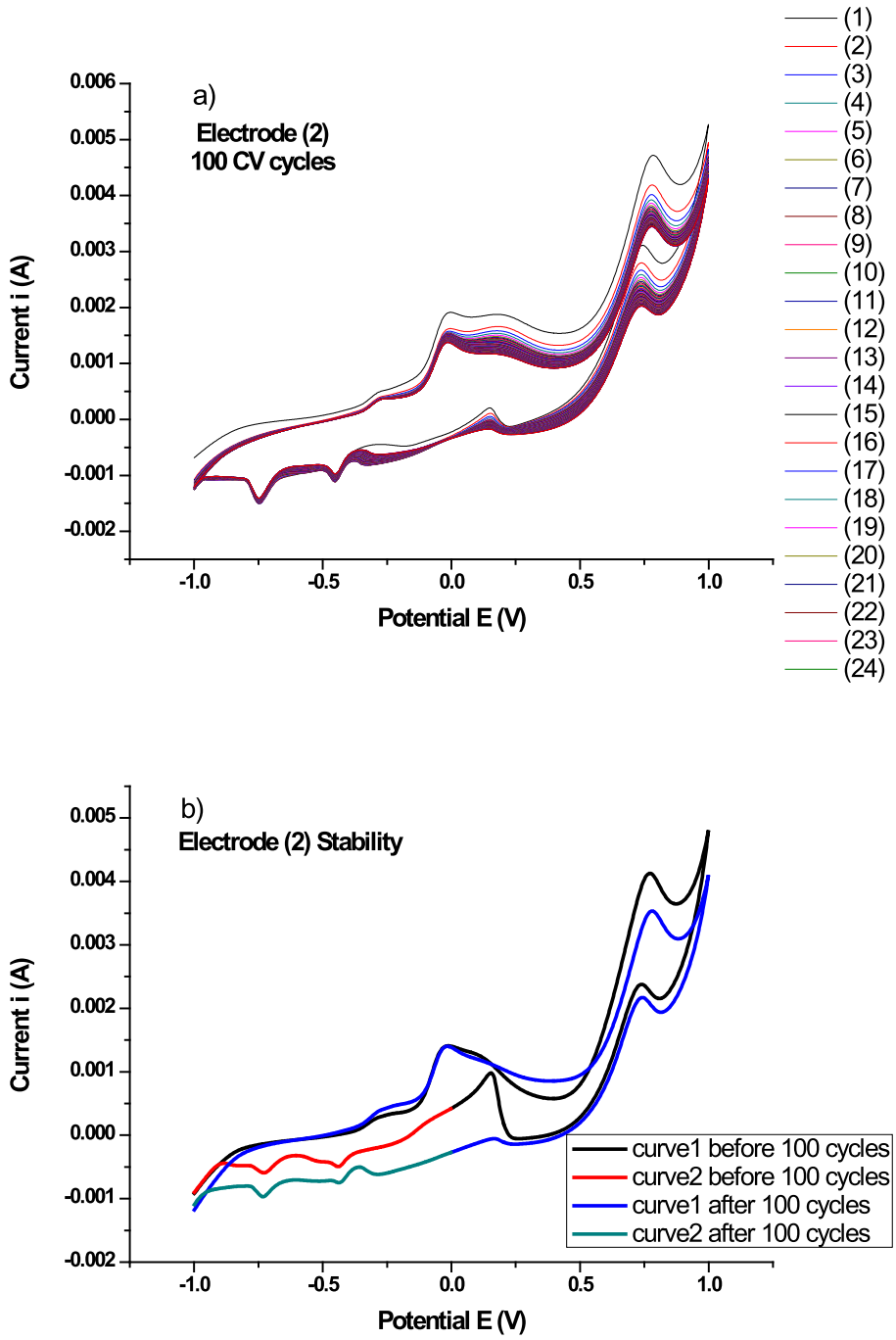

Fig. 7. (a) Stability of thiol modified electrode (2) in presence of glucose (33.82 mM) and 0.5 M NaOH for 100 cycles at scan rate 100 mV/s (b) Comparison of electroactivity of electrode (2) before and after 100 cycles in NaOH 0.5 M and glucose 33.82 mM at scan rate 50 mV/s.

is increased by 21.6 % for peak A1 at − 266.4 mV and no change at peak A2 at − 16.17 mV, thus the electroactivity of electrode is not decreased. On the other hand, the decrease at A3 indicated drop in the concentration of glucose left due to successful catalytic degradation of glucose using electrode (2) as a result of running 100 CV cycles. Electrode 2 is also stable upon storage compared to biosensors which can be subject to bio degradation of anchored glucose oxidase enzyme.

3.3.5. *Impedance study*

In order to further verify the possibility to develop glucose sensor, the electrochemical impedance spectra (EIS) techniques were measured for both electrodes (1) and (2) with a wide range of glucose concentrations [26]. Also, we considered working with (EIS) techniques to avoid the effect of interference from other molecules on the cyclic voltammetry peaks. Before electrochemical impedance study (EIS) experiments, the open-circuit potential, E_{OCP} was applied 300 s until a stable value is achieved. This method studies the amount of current flow and the value of resistance in presence and absence of glucose [31]. The electrochemical impedance measurements were fitted against equivalent electrical circuits EEC models A and B using electrode (2) and (1), Fig. 8a and b respectively [25]. The fitted EEC model A consists of two circuits connected in series, Fig. 8a. The first circuit consisted of a film resistance (Rf) in parallel with a constant phase element of film (CPEf) and a second circuit containing a charge-transfer resistance (Rct) in parallel with a constant phase double layer (CPEdl). The double layer capacitance (Cdl) can also be calculated from the values of Rct, the

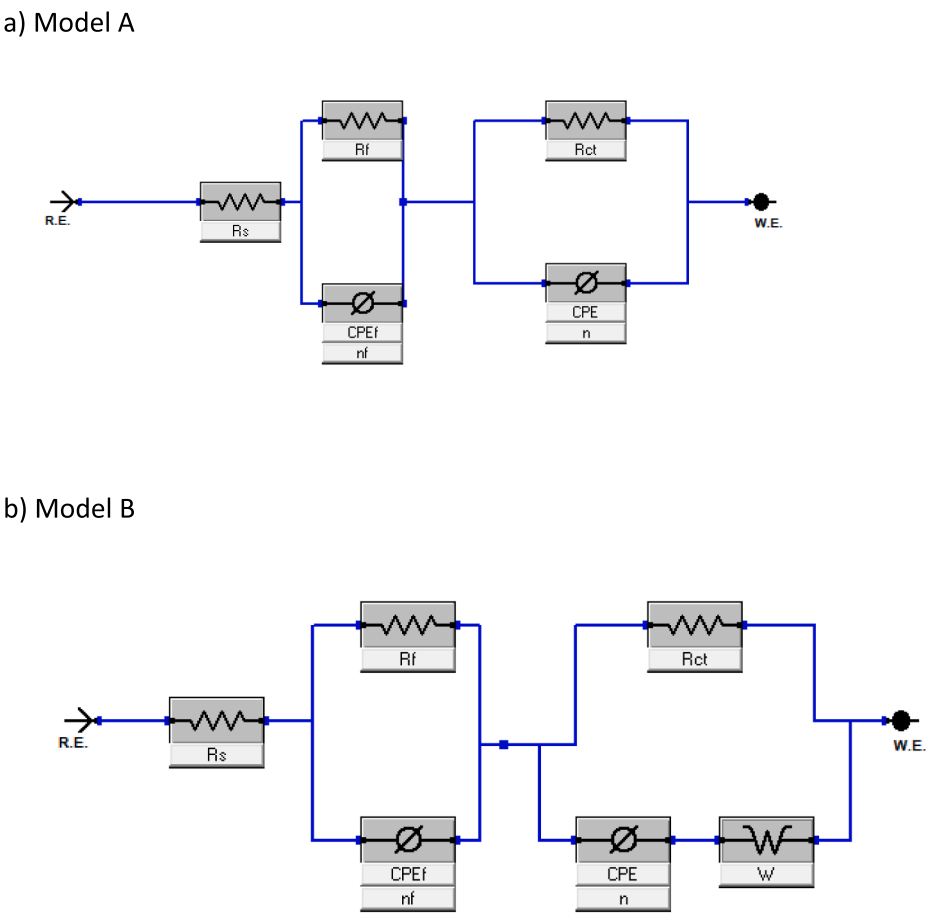

Fig. 8. (a) The best-fitted equivalent electrical circuit Model A for electrode (2) (b) The best-fitted equivalent electrical circuit Model B for electrode (1).

impedance of CPEdl (ZCPE), and the exponents of CPEdl (n) [25]. The EEC model B (Fig. 8b) contains two time constants similarly to Model A but has an additional diffusion component "Warburg impedance" (W) connected in parallel with a constant phase element (CPE).

The impedance data using electrode (1) with glucose solution of different concentrations, were fitted by Model B. The Nyquist plots were shown in Fig. 9a. While the impedance measurements using electrode (2) were fitted by Model A and the plots were shown in Fig. 9b. While Fig. 9c is an overlay figure of the impedance plots for better comparison of the performance of the two electrodes (**1**) and (**2**).

The Bode plots fitted by equivalent circuits model B and A were shown in Fig. 10a and b for electrodes (1) and (2) respectively.

The influence of glucose concentration is well reflected through Rs/Rso as it is directly proportional to glucose concentration up to 20 mM with a sensitivity of 0.0072 Ω mM^{-1} (28.8 mΩ mM^{-1} cm^{-2}) (R^2 = 0.9907) for electrode (1) and up to concentration 20 mM with a sensitivity of 0.0041 mM^{-1} (16.4 mΩ mM^{-1} cm^{-2}), $R^2 = 0.9907$ for electrode (2), Fig. 11a and 11b. The plots of Rs/Rs0 vs glucose concentration mM gave better correlation than the plots of Rct/Rct0 vs glucose concentration mM with both electrodes. Alternatively, a calibration curves can be obtained based on the change in the complex impedance Z (ohm) at a single frequency. Bode plot (Fig. 11c) showed that the complex impedance Z (ohm) increased systemically at a frequency of 2 Hz for electrode (1) with the increase in glucose concentration up to 15 mM. The sensitivity was 22.80 Ω mM^{-1} (91.2 Ω mM^{-1} cm^{-2}), $R^2 = 0.9671$. While the plot of Z (ohm) versus glucose concentration (mM) at frequency 0.2 Hz for electrode (2), showed a sensitivity of 0.5668 Ω mM^{-1} (2.27 Ω mM^{-1} cm^{-2}) with $R^2 = 0.9592$ (Fig. 11d). The dynamic range 1–15 mM. The limit of detections was 1 mM for both electrode (1) and (2).

The single-frequency approach has been reported as an alternative for the change of charge transfer resistance Rct with the increased concentration [26,30]. However, the results demonstrated that although Rs changed as function of glucose concentration could be exploited to quantify glucose, it is a time-consuming and laborious process, since the equivalent circuit EEC should be well fitted to obtain the resistance values involved in the circuit. To our knowledge, there is a few reports that used single-frequency approach to glucose quantification. Finally, Table 2 shows comparison between electrodes (1) and (2) and other reported glucose sensors in terms of linear range and limit of detection LOD. Both electrode (1) and (2) have the advantage of ease of preparation, low cost-effective materials, wide dynamic range, high sensitivity, high linearity, and short detection time. In addition, the advantage of EIS is its probing relaxation phenomena for a wide frequency range. This makes measurements very precise since the response can be indefinitely steady and thus can be averaged over a long period [26]. The electrodes are compared with other biosensors using glucose oxidase[32–34]; and with other sensors graphene - copper oxides nanoparticles [26] and graphene – copper nanoparticles [28].

4. Conclusion

We successfully developed new sensor based Gold/Graphene/Copper heterogeneous films. The obtained materials were functionalized using 4-NTP molecules. The sensors prepared are nano-gold/graphene/copper film (Au-7.5 nm/Gr/Cu) electrode (1) and its thiol (4-NTP) modified electrode (2) (4-NTP/Au-7.5 nm/Gr/Cu). The sensors were successfully characterized using SEM and SERS techniques. SERS confirmed of optical enhancement due to presence of active sites into the surface of gold nanostructures. The sensors were used in the detection of glucose using electrochemical measurement. Cyclic voltammetry

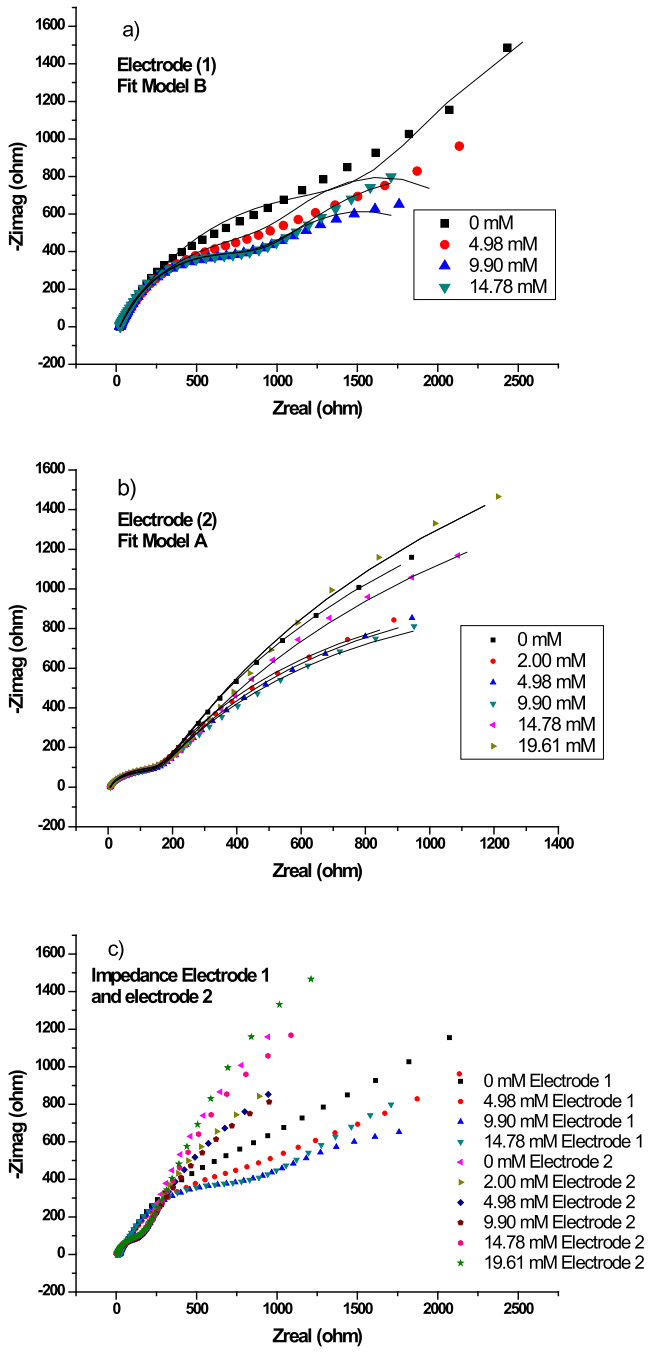

Fig. 9. Electrochemical oxidation of glucose at different concentration mM, in 0.5 M NaOH solution: (a) Nyquist plot with fitting using equivalent circuit Model B for electrode (1); (b) Nyquist plot fitted using equivalent circuit Model A for electrode (2); (c) Comparison between Nyquist plot of electrode (1) and electrode (2).

showed a high increase in the fast charge–discharge. In addition, Nyquisit plot proved that resistance is smaller in functionalized surface than without 4-NTP molecules. Both electrodes were tested for the determination of glucose (mM). The sensor property of electrode (2) is higher than electrode (1). This can be explained due to the functionalization with thiol groups of nanogold surface in the case of electrode (2). The dynamic range is 2.0–19.6 mM (36.0—353.2 mg/dL) of glucose for electrode 1 while it is 2.0–29.1 mM (36.0–524.9 mg/dL) of glucose for electrode 2. The sensitivity obtained by cyclic voltammetry was 179.6 mA/mM.cm^2 and 420.8 mA/mM.cm^2 for electrode (1) and (2) respectively. The anodic peak current intensity A3, in presence of glucose

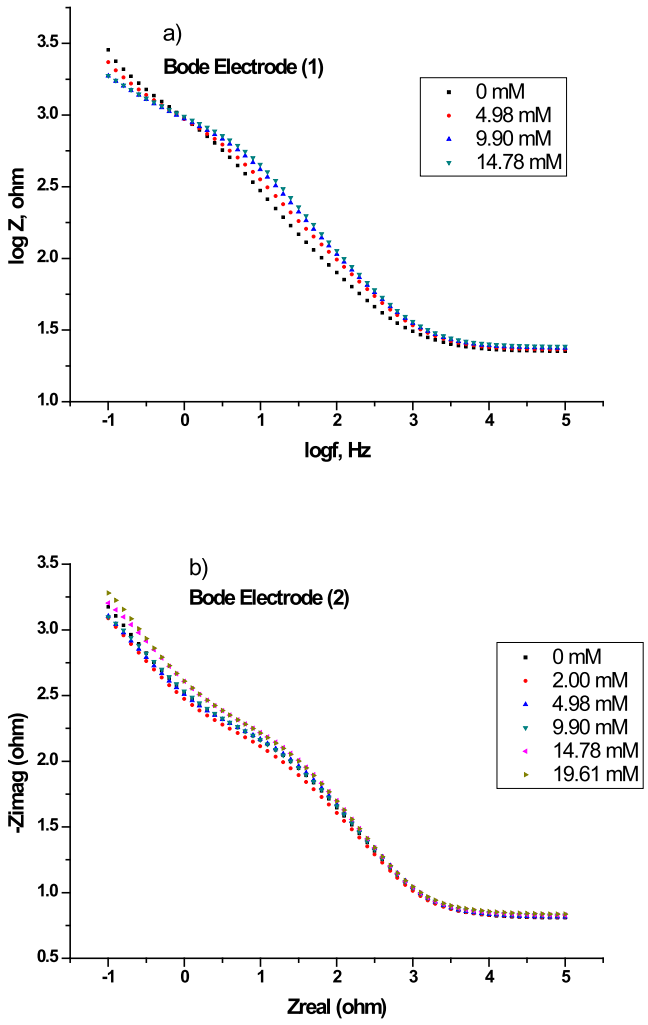

Fig. 10. (a) Bode plot for electrode (1) and (b) Bode plot for electrode (2) in NaOH (0.5 M) at different glucose concentration (mM).

(33.82 mM) in 0.5 M NaOH, retained 85.54% of its original value after 100 cycles. The determination of glucose was also studied by impedimetric techniques.

CRediT authorship contribution statement

Chawki Awada: Conceptualization, Methodology, Formal analysis, Investigation, Resources, Data curation, Writing – original draft, Writing – review & editing, Supervision, Funding acquisition. **Hassan H. Hammud:** Methodology, Formal analysis, Investigation, Resources, Writing – original draft, Writing – review & editing, Supervision, Funding acquisition. **Hawra A. Bukhamsin:** Formal analysis, Investigation. **Dolayl E. Al-Hudairi:** Formal analysis, Investigation. **Francesco Ruffino:** Methodology, Formal analysis, Resources, Data curation, Writing – original draft, Writing – review & editing, Supervision, Funding acquisition.

Declaration of Competing Interest

The authors declare that they have no known competing financial interests or personal relationships that could have appeared to influence the work reported in this paper.

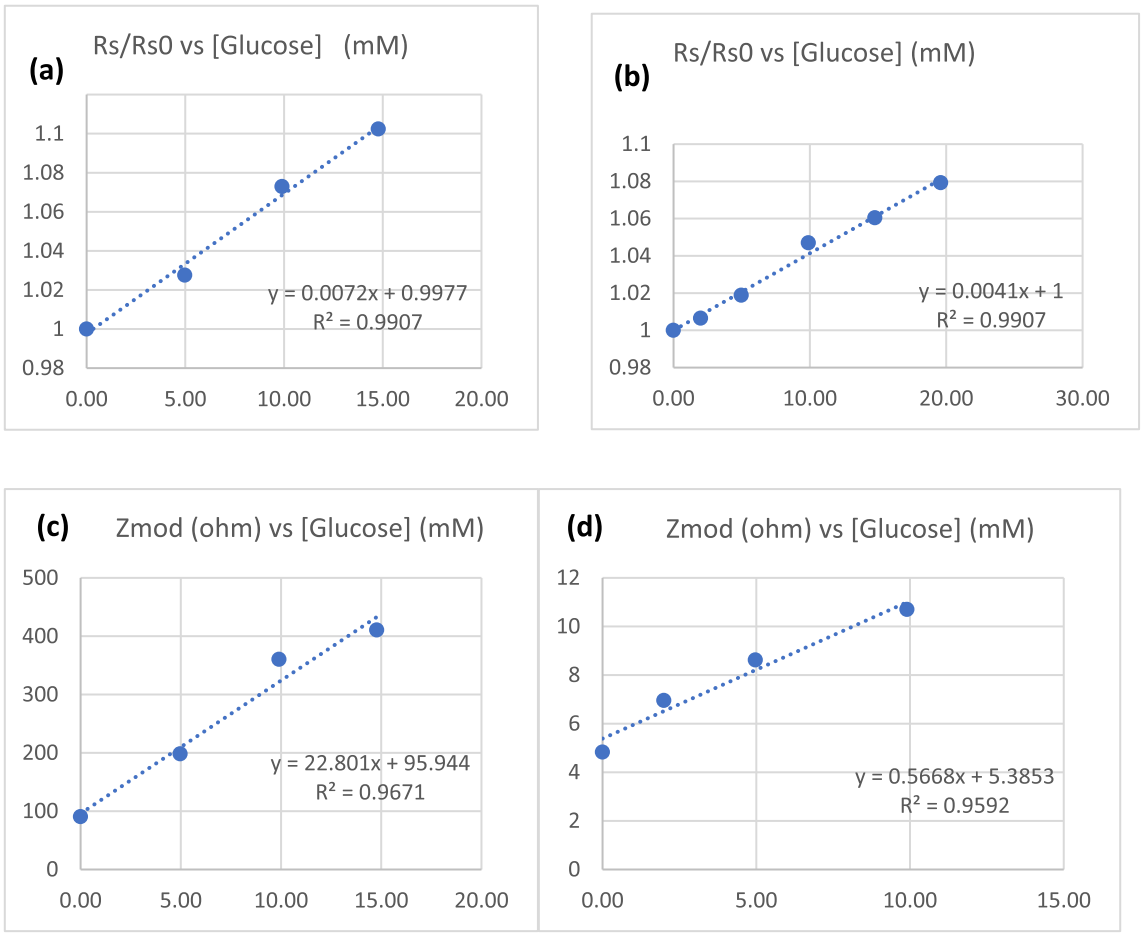

Fig. 11. (a) Calibration curves obtained at different concentration of glucose (mM) in 0.5 M NaOH a) for electrode (1) from the normalized Rs by fitting the data of Nyquist plot with equivalent circuit Model B; b) for electrode (2) from the normalized Rs by fitting the data of Nyquist plot with equivalent circuit Model A; c) for electrode (1) from Bode plot of the complex impedance at a frequency of 2 Hz for electrode (1); d) for electrode (2) from Bode plot of the complex impedance at a frequency of 0.2 Hz.

Table 2
Performance comparison of the proposed sensor to the previous works.

Material	Detection Method	Linear Range (mM)	Sensitivity	Limit of Detection LOD (mM)	Reference
(Au-7.5 nm/Gr/Cu) (1)	Cyclic voltammetric	1–20	179.6 μA/mM.cm^2	0.5	This work
(4-NTP/Au-7.5 nm/Gr/Cu) (2)	Impedimetric	1–29.1	420.8 μA/mM.cm^2	0.5	
(Au-7.5 nm/Gr/Cu) (1)		1–15	91.2 Ω mM^{-1} cm^{-2}	1.0	
(4-NTP/Au-7.5 nm/Gr/Cu) (2)		1–10	2.27 Ω mM^{-1} cm^{-2}	1.0	
Nafion/GOx/ZnO/ITO	Amperometric	0.05–1.0	48.75 μA/mM.cm^2	0.06	[32]
Nafion-Glucose oxidase-Zinc oxide nanorods-ITO glass		1–20	3.87 μA/mM.cm^2		
RGO–GOx	Amperometric	0.1–27	1.85 μAmM^{-1}cm^{-2}	0.1	[33]
Graphene–glucose oxidase					
Ppy-Gr-GOD	Amperometric	2–40 × 10^{-3} M	–	0.003	[34]
Polypyrrole-graphene-glucose oxidase					
CuO/Gr	Cyclic voltammetric	5–14	37.63 μA/mM.cm^2	0.005	[26]
Graphene-copper oxide nanoparticles					
Cu/Gr	Amperometric	0.05–4.5	–	0.0005	[28]
Graphene – copper nanoparticles					

Data availability

Data will be made available on request.

Acknowledgments

F. R. thanks the support by the projects: (1) Programma di Ricerca di Ateneo UNICT 2020-22 linea 2; (2) European Union (Next Generation EU), through the MUR-PNRR project SAMOTHRACE (ECS00000022); (3) PNRR MUR project PE0000023-NQSTI

Appendix A. Supplementary material

S**upplementary data to this article can be found online at https://doi.org/10.1016/j.apsusc.2023.158012.

References

[1] S. Petralia, E.L. Sciuto, S. Conoci, A novel miniaturized biofilter based on silicon micropillars for nucleic acid extraction, Analyst 142 (2017) 140–146, https://doi.org/10.1039/C6AN02049F.

[2] Y. Zeng, Z. Zhu, D. Du, Y. Lin, Nanomaterial-based electrochemical biosensors for food safety, J. Electroanal. Chem. 781 (2016) 147–154, https://doi.org/10.1016/j.jelechem.2016.10.030.

[3] M. Medina-Sánchez, C. Mayorga-Martinez, T. Watanabe, T. Ivandini, Y. Honda, F. Pino, K. Nakata, A. Fujishima, Y. Einaga, A. Merkoçi, Microfluidic platform for environmental contaminants sensing and degradation based on boron-doped diamond electrodes, Biosens. Bioelectron. 75 (2016) 365–374, https://doi.org/10.1016/j.bios.2015.08.058.

[4] Y.J. Lee, S.J. Park, K.-S. Yun, J.Y. Kang, S.H. Lee, Enzymeless glucose sensor integrated with chronically implantable nerve cuff electrode for in-situ inflammation monitoring, Sensors Actuators B Chem. 222 (2016) 425–432, https://doi.org/10.1016/j.snb.2015.08.091.

[5] X. Kang, Z. Mai, X. Zou, P. Cai, J. Mo, A sensitive nonenzymatic glucose sensor in alkaline media with a copper nanocluster/multiwall carbon nanotube-modified glassy carbon electrode, Anal. Biochem. 363 (2007) 143–150, https://doi.org/10.1016/j.ab.2007.01.003.

[6] A.A. Saei, J.E.N. Dolatabadi, P. Najafi-Marandi, A. Abhari, M. de la Guardia, Electrochemical biosensors for glucose based on metal nanoparticles, TrAC, Trends Anal. Chem. 42 (2013) 216–227, https://doi.org/10.1016/j.trac.2012.09.011.

[7] T. Jufík, P. Podešva, Z. Farka, D. Kovář, P. Skládal, F. Foret, Nanostructured gold deposited in gelatin template applied for electrochemical assay of glucose in serum, Electrochim. Acta. 188 (2016) 277–285, https://doi.org/10.1016/j.electacta.2015.12.009.

[8] R.L. McCreery, Advanced carbon electrode materials for molecular electrochemistry, Chem. Rev. 108 (2008) 2646–2687, https://doi.org/10.1021/cr068076m.

[9] M. Zhou, Y. Zhai, S. Dong, Electrochemical Sensing and Biosensing Platform Based on Chemically Reduced Graphene Oxide, Anal. Chem. 81 (2009) 5603–5613, https://doi.org/10.1021/ac900136z.

[10] P.T. Yin, T.-H. Kim, J.-W. Choi, K.-B. Lee, Prospects for graphene–nanoparticle-based hybrid sensors, Phys. Chem. Chem. Phys. 15 (2013) 12785–12799, https://doi.org/10.1039/C3CP51901E.

[11] F. Ruffino, V. Torrisi, G. Marletta, M.G. Grimaldi, Growth morphology of nanoscale sputter-deposited Au films on amorphous soft polymeric substrates, Appl. Phys. A. 103 (2011) 939–949, https://doi.org/10.1007/s00339-011-6413-1.

[12] G.B.B.E.A. Brandes (Ed.), Smithells Metals Reference Book, 7th Editio, Elsevier, Butterworth-Heinemann, 1998.

[13] S. Wang, Y. Zhang, N. Abidi, L. Cabrales, Wettability and Surface Free Energy of Graphene Films, Langmuir 25 (2009) 11078–11081, https://doi.org/10.1021/la901402f.

[14] M. Lucchesi, G. Privitera, M. Labardi, D. Prevosto, S. Capaccioli, P. Pingue, Electrostatic force microscopy and potentiometry of realistic nanostructured systems, J. Appl. Phys. 105 (2009) 54301, https://doi.org/10.1063/1.3082125.

[15] Y. Bai, F. Feng, L. Zhao, C. Wang, H. Wang, M. Tian, J. Qin, Y. Duan, X. He, Aptamer/thrombin/aptamer-AuNPs sandwich enhanced surface plasmon resonance sensor for the detection of subnanomolar thrombin, Biosens. Bioelectron. 47 (2013) 265–270, https://doi.org/10.1016/j.bios.2013.02.004.

[16] C. Awada, M.M.B. Abdullah, H. Traboulsi, C. Dab, A. Alshoaibi, SARS-CoV-2 Receptor Binding Domain as a Stable-Potential Target for SARS-CoV-2 Detection by Surface—Enhanced Raman Spectroscopy, Sensors 21 (2021) 4617, https://doi.org/10.3390/s21134617.

[17] C. Dab, C. Awada, A. Merlen, A. Ruediger, Near-field chemical mapping of gold nanostructures using a functionalized scanning probe, Phys. Chem. Chem. Phys. 19 (2017) 31063–31071, https://doi.org/10.1039/C7CP06004A.

[18] J. Hernández, J. Solla-Gullón, E. Herrero, A. Aldaz, J.M. Feliu, Methanol oxidation on gold nanoparticles in alkaline media: Unusual electrocatalytic activity, Electrochim. Acta. 52 (2006) 1662–1669, https://doi.org/10.1016/j.electacta.2006.03.091.

[19] M. Graf, M. Haensch, J. Carstens, G. Wittstock, J. Weissmüller, Electrocatalytic methanol oxidation with nanoporous gold: microstructure and selectivity, Nanoscale 9 (2017) 17839–17848, https://doi.org/10.1039/C7NR05124G.

[20] S. Yang, D.G.H. Hetterscheid, Redefinition of the Active Species and the Mechanism of the Oxygen Evolution Reaction on Gold Oxide, ACS Catal. 10 (2020) 12582–12589, https://doi.org/10.1021/acscatal.0c03548.

[21] I.M. Al-Akraa, A.M. Mohammad, M.S. El-Deab, B.E. El-Anadouli, Flower-shaped gold nanoparticles: Preparation, characterization, and electrocatalytic application, Arab. J. Chem. 10 (2017) 877–884, https://doi.org/10.1016/j.arabjc.2015.05.004.

[22] M.S. Ali Akbari, R. Bagheri, Z. Song, M.M. Najafpour, Oxygen-evolution reaction by nickel/nickel oxide interface in the presence of ferrate(VI), Sci. Rep. 10 (2020) 8757, https://doi.org/10.1038/s41598-020-65674-x.

[23] N. Schlegel, G.K.H. Wiberg, M. Arenz, On the electrooxidation of glucose on gold: Towards an electrochemical glucaric acid production as value-added chemical, Electrochim. Acta. 410 (2022), 140023, https://doi.org/10.1016/j.electacta.2022.140023.

[24] G. Moggia, T. Kenis, N. Daems, T. Breugelmans, Electrochemical Oxidation of d-Glucose in Alkaline Medium: Impact of Oxidation Potential and Chemical Side Reactions on the Selectivity to d-Gluconic and d-Glucaric Acid, ChemElectroChem 7 (2020) 86–95, https://doi.org/10.1002/celc.201901592.

[25] H.H. Hammud, S.A. Maache, N. Al Otaibi, N.S. Sheikh, An Integrated Experimental and Theoretical Studies on the Corrosion Inhibition of Carbon Steel by Harmal Extracts, Molecules 27 (2022), https://doi.org/10.3390/molecules27217250.

[26] F. Foroughi, M. Rahsepar, M.J. Hadianfard, H. Kim, Microwave-assisted synthesis of graphene modified CuO nanoparticles for voltammetric enzyme-free sensing of glucose at biological pH values, Mikrochim. Acta. 185 (2017) 57, https://doi.org/10.1007/s00604-017-2558-8.

[27] N. Alotaibi, H.H. Hammud, N. Al Otaibi, T. Prakasam, Electrocatalytic Properties of 3D Hierarchical Graphitic Carbon-Cobalt Nanoparticles for Urea Oxidation, ACS, Omega 5 (2020) 26038–26048, https://doi.org/10.1021/acsomega.0c03477.

[28] J. Luo, S. Jiang, H. Zhang, J. Jiang, X. Liu, A novel non-enzymatic glucose sensor based on Cu nanoparticle modified graphene sheets electrode, Anal. Chim. Acta. 709 (2012) 47–53, https://doi.org/10.1016/j.aca.2011.10.025.

[29] H. Grönbeck, A. Curioni, W. Andreoni, Thiols and Disulfides on the Au(111) Surface: The Headgroup−Gold Interaction, J. Am. Chem. Soc. 122 (2000) 3839–3842, https://doi.org/10.1021/ja993622x.

[30] H.H. Hammud, N. Alotaibi, N. Al Otaibi, A. Aljaafari, F. Ahmed, A. Azam, T. Prakasam, Hierarchical Porous Carbon Cobalt Nanocomposites-Based Sensor for Fructose, Chemosensors. 9 (2021), https://doi.org/10.3390/chemosensors9010006.

[31] N. Al Otaibi, H.H. Hammud, Corrosion Inhibition Using Harmal Leaf Extract as an Eco-Friendly Corrosion Inhibitor, Molecules 26 (2021), https://doi.org/10.3390/molecules26227024.

[32] N.S. Ridhuan, K. Abdul Razak, Z. Lockman, Fabrication and Characterization of Glucose Biosensors by Using Hydrothermally Grown ZnO Nanorods, Sci. Rep. 8 (2018) 13722, https://doi.org/10.1038/s41598-018-32127-5.

[33] B. Unnikrishnan, S. Palanisamy, S.-M. Chen, A simple electrochemical approach to fabricate a glucose biosensor based on graphene–glucose oxidase biocomposite, Biosens. Bioelectron. 39 (2013) 70–75, https://doi.org/10.1016/j.bios.2012.06.045.

[34] S. Alwarappan, C. Liu, A. Kumar, C.-Z. Li, Enzyme-doped graphene nanosheets for enhanced glucose biosensing, J. Phys. Chem. C. 114 (2010) 12920–12924, https://doi.org/10.1021/jp103273z.